Structural and magnetic investigations of a binuclear coordination compound of dysprosium(III) dinitrobenzoate

B.S. Sran, J.F. Gonzalez, V. Montigaud, Boris Le Guennic, Fabrice Pointillart, O. Cador, G. Hundal

Structural and Magnetic Investigations of a Binuclear Coordination Compound of Dysprosium (III) Dinitrobenzoate

Received 00th January 20xx,
Accepted 00th January 20xx

DOI: 10.1039/x0xx00000x

www.rsc.org/

Balkaran Singh Sran,[a] Jessica Flores Gonzalez,[b] Vincent Montigaud,[b] Boris Le Guennic,[b] Fabrice Pointillart,*[b] Olivier Cador,*[b] Geeta Hundal*[a]

A centro-symmetric binuclear compound of formula $[Dy(\mathbf{L})\cdot(CH_3COO)_2\cdot(H_2O)_2]_2$ (**1**) was isolated from the reaction between the 2,4-dinitrobenzoate anion (**L**) and the tris(acetate) of Dy(III). Single crystal diffraction studies reveal a μ_1-κ^2, η^1:η^1 chelating binding mode of **L** while the binuclear compound is owing to the two bridging (μ_2-κ^3, η^1:η^2) acetate anions. The nona-coordinated sphere of each Dy(III) ion is filled with a chelating (κ^2, η^1: η^1) acetate anion and two terminal water molecules. Static magnetic measurements combined with ab initio SA-CASSCF/RASSI-SO calculations lead to two intramolecular competitive interactions i.e. ferromagnetic exchange interactions (0.04 cm^{-1}) and antiferromagnetic dipolar interactions (-0.5 cm^{-1}). Finally dynamic magnetic measurements revealed a Single-Molecule Magnet behaviour in zero-applied magnetic field with an effective energy barrier Δ = 31(2)K and τ_0 = 7(3)x10^{-6} s through Orbach and Quantum Tunnelling of the Magnetization relaxation mechanisms.

Introduction

Since the discovery of the first lanthanide Single-Molecule Magnet (SMM),[1] the design and study of such objects have generated considerable fascination. Indeed, the combination of high magnetic moment and strong magnetic anisotropy makes such ions ideal candidates for the observation of slow relaxation of their magnetization leading to the possible measurement of magnetic bistability at low temperature and thus potential applications in high density data storage.[2-4] Since their performance was stagnated for more than a decade with a record of blocking temperature at 14 K,[5,6] these objects were also dedicated to other potential applications such as quantum computing and spintronics.[7-11] Last year, the interest for SMM in the high density data storage and their slow magnetic relaxation got a fresh breath with the discovery of a mononuclear Dysprosium compound which displayed high blocking temperature close to the liquid nitrogen temperature.[12-14]

Many works on mononuclear SMMs highlighted that a fine control of the coordination environment of the single magnetic centre (i.e. tuning the crystal field of the lanthanoid) may lead to the magnification of the SMM properties. However, many questions still remain on the understanding and control of the relaxation mechanisms involved in these coordination compounds. The advances made from both experimental and theoretical fields allowed the emergence of more sophisticated architectures composed by several magnetic centers.[15-18] Efforts were then focused on the understanding of magnetic interactions involved in these polynuclear compounds and their influence on the relaxation dynamics. In particular, binuclear systems have proven to be the perfect subject for the investigation of the influence of intramolecular magnetic interactions on the relaxation dynamics, motivating the present work.[19-23]

The choice of the nature of the ligand is crucial to impose the right crystal field and electronic distribution around the lanthanide ions and to induce an adequate energy splitting of the ground multiplet state for the observation of slow magnetic relaxation.[24] Thus, it was already observed that an appropriate electrostatic distribution in the vicinity of the magnetic ion could be obtained with the association of carboxylate-based ligands and lanthanide ions leading to a well-isolated ground state and apparition of a slow magnetic relaxation.[25-29]

Following this idea, some of us started to associate dinitrobenzoate ligand to lanthanide ions to elaborate luminescent SMMs. Both 2,4-dinitrobenzoate (Scheme 1) and 3,5-dinitrobenzoate permitted the observation of slow magnetic relaxation in 1D polymeric compounds of Nd(III) ion.[30-31]

In the present paper, we present the association of the Dy(III) ion with the 2,4-dinitrobenzoate anion (**L**) giving the formation of a binuclear compound of formula $[Dy(\mathbf{L})\cdot(CH_3COO)_2\cdot(H_2O)_2]_2$ (**1**). Its structural and magnetic properties were studied and the latter were rationalized by SA-CASSCF/RASSI-SO calculations.

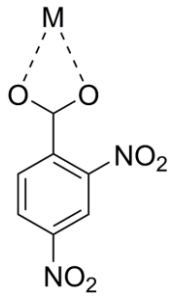

Scheme 1. Chelating binding mode of ligand (**L**) (μ1-κ2, η1:η1).

Experimental Section

Materials and physical measurements

[a] *Department of Chemistry, UGC sponsored centre of advance studies-II, Guru Nanak Dev University, Amritsar-143005, Punjab, India.*
[b] *Univ Rennes, CNRS, ISCR (Institut des Sciences Chimiques de Rennes) - UMR 6226, 35000 Rennes, France.*

Electronic Supplementary Information (ESI) available: structural information, thermal analysis, static magnetic measurements and computational data. CCDC No for complex **1** is 1584540.See DOI: 10.1039/x0xx00000x

All the reagents were commercially available and used as received. C, H, N elemental analyses were obtained with a CHNS-O analyser flash-EA-1112 series. The IR spectra of all compounds were recorded on Perkin ELMER FTIR spectrometer in the range 4000-400 cm^{-1}. Thermogravimetric analysis (TGA) data were collected on a NetzschTG-209 instrument. The dc magnetic susceptibility measurements were performed on solid polycrystalline sample with a Quantum Design MPMS-XL SQUID magnetometer between 2 and 300 K in an applied magnetic field of 0.2 kOe in the 2-20 K temperature range, 2 kOe in the 2-20 K temperature range and 10 kOe between 80 and 300 K. These measurements were all corrected for the diamagnetic contribution as calculated with Pascal's constants. Magnetization measurements in alternating field at various frequencies have been performed with 3 Oe oscillating field amplitude. The X-ray powder diffraction (PXRD) measurements were recorded on a Bruker D8 Focus X-ray diffractometer with CuKα radiation (λ = 1.54056 Å).

General Procedure for synthesis of the compound $Dy(L)\cdot(CH_3COO)_2\cdot(H_2O)_2]_2$ (1).

2, 4-Dinitrobenzoic acid (1 mmol, 0.21 g) was dissolved into a minimum quantity of acetonitrile. To an aqueous solution of $Dy(CH_3COO)_3\cdot 4H_2O$ (0.411 g, 1 mmol), 2-3 drops of 0.1 N NaOH was added and the solution was stirred for half an hour. The solution of 2, 4-Dinitrobenzoic acid was added to this solution dropwise with continuous stirring and after addition, the solution was stirred for 2 hours. The resulting solution was allowed to slowly evaporate. Colourless crystals of **1** were obtained within 10 days. M.p. > 300 °C Anal. Calcd for $C_{22}H_{26}N_4O_{24}Dy_2$ (%): C, 25.04; H, 2.48; N, 5.31; Found: C, 24.98; H, 2.56; N, 5.24. IR (cm^{-1}) selected bonds: ν = 3348 (b) (O-H), 3060 (m) (Ar-H), 1546 (w) $(COO\text{-})_{asym}$, 1377 (s) $(COO\text{-})_{sym}$, 1417 (w) (C=C), 1349 (m) (N-O), 617 (w) (M-O). (b = broad, m = medium, s = strong, w = weak).

X-ray crystallography

X-ray data of **1** were collected on a Bruker Apex-II CCD diffractometer using Mo Kα radiation (λ = 0.71069 Å) at room temperature and processed by SAINT. Lorentz and polarization effects and empirical absorption corrections were applied using SADABS from Bruker. The structure was solved by direct methods, using SHELX-2014[32] and refined by full-matrix least squares refinement methods based on F^2, using SHELX-2017.[33] All non-hydrogen atoms were refined anisotropically. All hydrogen atoms were fixed geometrically with their U_{iso} values 1.2 times that of the phenylene carbons and 1.5 times that of the methyl group. The hydrogen atoms of the water molecules were located from the difference Fourier synthesis and were refined isotropically with a distance of 0.82 Å with U_{iso} values 1.2 times that of their carrier oxygen atoms. All calculations were performed using the WinGX package.[34]

Hirshfeld analysis

Hirshfeld surface analysis[35] was carried out using crystal explorer 3.1 software.[36] It is a technique to find out intermolecular interactions or closest contacts like H···O/ H···O, H···H, O···O, N···H/H···N and π···π (C···C) to support the X-ray data.[37] The results of crystal packing interactions are displayed into a 2D fingerprint plot[38] and single 3D surface by this software. [39] The 3D d_{norm} surfaces are charted over a fixed colour scale of 1.25 (red) to 1.52 Å (blue), shape index and curvedness are mapped in the colour range of -1.0 to 1.0 Å and 4.0 to 0.4 Å, respectively. The 2D fingerprint plots are displayed by using the extended 0.4–2.8 Å view, with the d_e and d_i distance scales displayed on the graph axes.

Computational details

The atomic positions were extracted from the X-ray diffraction crystal structure of $[Dy(\mathbf{L})\cdot(CH_3COO)_2\cdot(H_2O)_2]_2$ (**1**). Calculations are performed on one magnetic centre while the other Dy(III) ion is replaced by a diamagnetic Y(III) ion using the State-Averaged Complete Active Space Self-Consistent Field approach with restricted-active-space-state-interaction method (SA-CASSCF/RASSI-SO), as implemented in the MOLCAS quantum-chemistry package (versions 8.0).[40] The relativistic effects are treated in two steps on the basis of the Douglas–Kroll-Hess Hamiltonian. The scalar terms were included in the basis-set generation and were used to determine the CASSCF wavefunctions and energies.[41] Spin-orbit coupling was then added within the RASSI-SO method, which mixes the calculated CASSCF wavefunctions.[42,43] The resulting spin-orbit wavefunctions and energies were used to compute the magnetic properties and g-tensors of the ground state multiplet following the pseudospin S = 1/2 formalism, as implemented in the SINGLE-ANISO routine.[44,45] Then, the magnetic interactions are considered (within the Lines model) in the calculations through the POLY_ANISO routine.[46-48] The interaction Hamiltonian is built in the basis of the ground and first excited (spin-orbit) Kramers Doublets (KDs) of each magnetic centre resulting in the computation of $4^2 = 16$ exchange states (8 KDs, eq. 1).

$$\widehat{H} = -J_{12}^{dip}\hat{s}_1\hat{s}_2 - J_{12}^{exch}\hat{s}_1\hat{s}_2 \quad (1)$$

The dipolar interactions are computed exactly while the exchange interactions J^{exch} are fitted to reproduce the experimental results for the magnetic susceptibility. Cholesky decomposition of the bielectronic integrals was employed to save disk space and to speed up the calculations.[49] The active space consisted of the nine 4f electrons of the Dy(III) ion, spanning the seven 4f orbitals, that is, CAS(9,7)SCF. SA-CASSCF calculations were performed for all of the sextets (21 roots), all of the quadruplets (224 roots) and 300 out of the 490 doublets of the Dy(III) ion. Twenty-one sextets, 128 quadruplets and 107 doublets were mixed through spin–orbit coupling in the RASSI-SO routine. All atoms were described with ANO-RCC basis sets with the following contractions [8s7p4d3f2g1h] for Dy; [7s6p4d2f] for Y; [4s3p2d] for the O atoms of the first coordination sphere and [3s2p1d] for the C, N and the other O atoms and [2s] for the H atoms.[50,51]

Results and Discussion

Crystal structure description of $[Dy(L)\cdot(CH_3COO)_2\cdot(H_2O)_2]_2$ (1). **1** can be described as a dimeric compound (Fig. 1), crystallising in the orthorhombic centrosymmetric space group *Pbca* (Table 1).

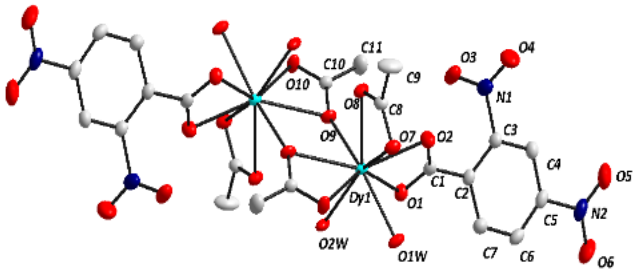

Fig 1. Dimeric unit of compound **1** with 30 % ellipsoid probability. Hydrogen atoms are omitted for clarity.

There is one crystallographically independent Dy(III) ion, one **L**, two acetate anions and two coordinated water molecules O1W and O2W in the asymmetric unit (Fig. S1). Each Dy(III) ion is nona-coordinated, with a distorted monocapped square anti-prismatic geometry (Fig. S2). Only a chelating mode of binding of the **L** (μ_1-κ^2, η^1:η^1) is present in this case with Dy1–O1 = 2.475(2) Å and Dy1–O2 = 2.472(2) Å, while the two acetate groups are chelating (κ^2, η^1: η^1) and bridging (μ_2-κ^3, η^1:η^2) tridentate, respectively, forming a dimer (Fig. 1). Average Dy–O (acetate) and Dy–OW distances are 2.457(2) Å and 2.343(2) Å (Table S1) respectively. The intramolecular Dy···Dy distance is 4.191(5) Å.

The crystal packing shows both intra- and inter-molecular H-bonding involving the water molecules and the acetate groups. Dimeric units are connected to one another through hydrogen bonding interactions O1W-H12W···O7, O1W-H11W···O1 and O2W-H21W···O10, resulting in the formation of a 1D chain as shown in Fig. 2. Further this chain structure is

Table 1. Crystallographic data for **1**.

Identification code	**1**
Empirical formula	C_{22} H_{26} Dy_2 N_4 O_{24}
Formula weight	1055.47
T(K)	296(2)
Crystal system	Orthorhombic
Space group	*P b c a*
Absorption coefficient (mm^{-1})	4.468
Crystal Size (mm^3)	0.20 x 0.20 x 0.10
a (Å)	13.8285(4)
b (Å)	8.9016(3)
c (Å)	27.5841(9)
α(°)	90°
β (°)	90°
γ (°)	90°
V ($Å^3$)	3395.49(19)
Z	4
F(0 0 0)	2040
Theta range for data collection	2.820 to 31.494°
Reflections collected	60008
Independent Reflections	5607
Final R indices	R1 = 0.0286, wR2 =0.0708
R indices (all data)	R1 = 0.0472, wR2 =0.0791
λ(Å)	0.71073
D_c(mg/m^3)	2.065
Data / restraints / parameters	5607 / 4/ 247
Completeness to theta = 25.242°	99.1%
Goodness of fit on F^2	1.064
CCDC No.	1584540

supported by lone Pair···π (LP···π) interactions between O6 of p-nitro group and aromatic ring from the adjacent dimeric units with centroid···O6 3.521 Å, α =61.21° , d_{offset}=1.695 and between O4 of O-nitro group and aromatic ring from the adjacent chain with centroid···O4 = 3.270 Å, α =67.77°, d_{offset}=1.123 (Fig S3). This relatively strong LP···π bonding[52] between the adjacent chains is further supported by weak H-bonding interactions C9-H9c···O6 between methyl of acetate groups, as shown in Fig S3. Important distances are given in Table S2 .

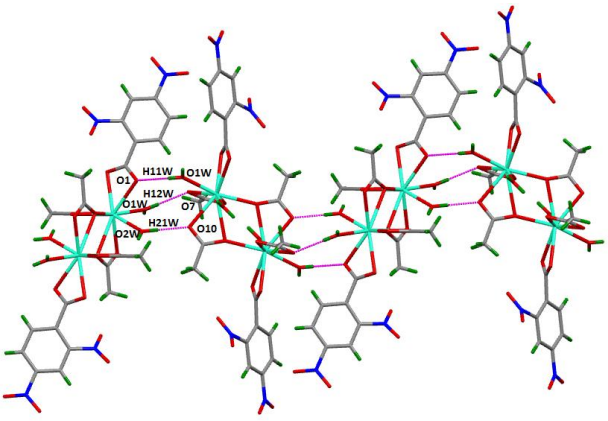

Fig 2. Showing intermolecular O(water)...O(carboxylate) hydrogen bonding (dotted magenta coloured lines) between dimers along the *b* axis.

To find out the role of nitro groups in the formation of the dimer, a CSD search using CSD version 5.39 updates (Aug 2018) was made which showed two complexes of Dy(III) benzoate (CSD ref codes- TEYBIF[53], BIHPAJ[54]) in the literature. Compound I has no water molecules in coordination and the structure is a 1D twisted ribbon, with Benzoate ion acting as doubly and triply bridging ligand and Dy…Dy distance as 3.95 Å while II is a zig zag 1D polymer having three coordinating water molecules, with monodentate and doubly bridging benzoate ion and Dy…Dy 5.577 Å .

The present complex has acetate as co-ligand (since structure of 2,4-DNB with Dy(III) is unknown) so comparing it with I shows that the first coordination sphere is more influenced by the acetate ion than by the nitro groups because in the present complex the acetate is behaving as a triply bridging ligand while DNB is simply a bidentate chelating ligand. Surprisingly the overall structure is merely a dimer with a comparable Dy…Dy distance, 4.19 Å. The propagation into a coordination polymer is curtailed by the non-bridging DNB ion, probably due to the steric hindrance from O-nitro group. Nitro groups, nevertheless, have significant role in the crystal structure due to H-bonding and LP···π interactions. However, the first coordination sphere, mode of coordination and Dy…Dy distance seem to be more influenced by the co-ligand (water or acetate) rather than the nitro groups.

Hirshfeld surface analysis was performed on the dimeric unit of **1** in order to give more insight about the intermolecular interactions occurring in the crystal. This surface is mapped using several criterions detailed in the experimental section and showed in Fig. 3. The d_{norm} function is highlighted from red, white to blue in an order of increasing distance with respect to the sum of the van der Waals radii and allows the identification and quantification of the atom/atom pairs participating to the surface. On the other hand, the curvedness map is most suited to identify the π···π interactions.

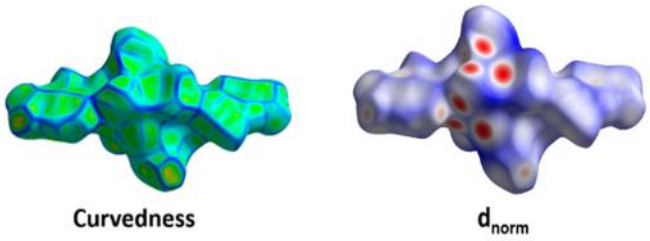

Fig 3. Hirshfeld surface mapped with d_{norm} and Curvedness for the dimeric unit of **1**.

The red areas found on the d_{norm} surface correspond to O···H/H···O interactions with neighbouring molecules. In order to give a quantitative description of the interactions involved in the Hirshfeld surface, 2D fingerprints of each pair are depicted in Fig S4 and S5. These values are obtained by integration of the surface area corresponding to an interaction over the total molecular Hirshfeld surface area. This decomposition highlights the strong contribution of the O···H/H···O pairs (48 %) in the intermolecular interactions. On the other hand, the low contribution of the C-C interactions (1%) and the absence of flat areas, on the curvedness representation, around the delocalized rings show the lack of π-stacking, ratifying the results of crystal packing.

IR spectroscopy, Thermogravimetric analysis, Powder X-ray Diffraction studies

Complex (**1**) was duly characterized by using IR spectrum, from the characteristic peaks of ν_{OH}, ν_{asym} and $\nu_{sym}(COO^-)$ and $\nu_{N\text{-}O}$. $\Delta\nu$ = 200 cm^{-1} ratifies the binding mode of L and acetate group (see supplementary section and Fig. S6 for details). TGA of (**1**) clearly shows the loss of four coordinated water molecules between 120 and 183 °C, after which the complex is stable up to 300 °C (Fig. S7, ESI). A comparison of the PXRD of the as-synthesized complex with that of the generated (from SCXRD) shows that the bulk compound consists of a single phase only (Fig. S8).

Magnetic Properties

Static magnetic measurements. The static magnetic properties were determined measuring the thermal dependence of the magnetic susceptibility (χ_M) between 2 and 300 K (Fig. 4). At room temperature, the χ_MT value (27.96 cm^3 K mol^{-1}) is close to the value expected of 28.4 cm^3 K mol^{-1} for two isolated Dy(III) ions ($^6H_{15/2}$ and g_J= 4/3).[55] On cooling, χ_MT remains constant down to 100 K and then monotonically decreases to reach a minimum of 17.33 cm^3 K mol^{-1} at 2 K. This decrease, more abrupt at low temperatures, is due to the combination of the thermal depopulation of the stark sublevels at high temperatures and weak antiferromagnetic interactions at low temperatures. At 2K, the field dependence of the magnetization shows a classical behaviour with a value of 10 Nβ at 50 KOe. This value is far from expected for the multiplet ground state $^6H_{15/2}$ (20 Nβ) but perfectly matches with a Ising ground state (10 Nβ) which corresponds to the stabilization of the Kramers doublet M_J = ±15/2.

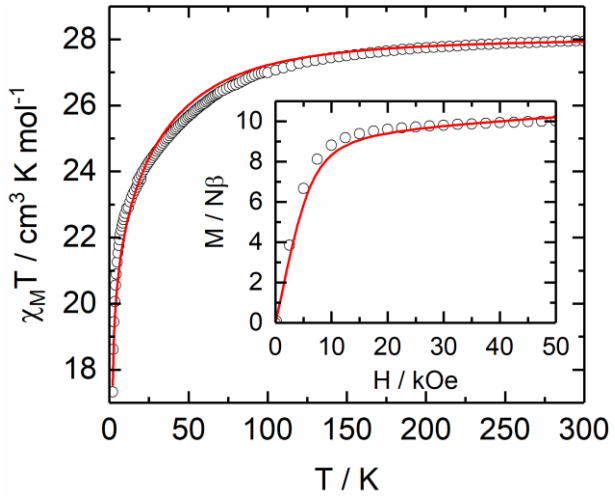

Fig 4. Thermal dependence of χ_MT for **1** (open circles). The inset corresponds to the field dependence of magnetization at 2 K (black circles). The red lines represent the best simulated curves from ab initio calculations.

Dynamic magnetic measurements. Dynamic magnetic measurements have been performed under zero dc magnetic field for temperatures between 2 and 9 K. The variations in frequency of the out-of-phase component, χ_M'', of the molar

magnetic susceptibility at various temperatures is represented on Fig. 5a with a clear frequency dependence below 9 K. Below 7 K, a maximum shifts in the 1-1000 Hz window. The relaxation time (τ) have been extracted at each temperature in fitting simultaneously the frequency dependence of χ_M' (in-phase) and χ_M'' with an extended Debye model (see SI, Fig S9-11, Table S3).[56] One can find advantages with such fitting procedure instead of pointing the maxima on χ_M'' vs. frequency curves: 1) The α value which describes the dispersion of the relaxation time is accessible and, in principle, should be close to zero since we expect to have a single relaxation time. 2) The fitting procedure allows also to verify that the high frequency limit of the magnetic susceptibility (χ_S) is very small with respect to the low frequency limit (χ_T) so 100% of the dysprosium centres relax at the same frequency. The temperature dependence of the relaxation time (τ) follows a modified Arrhenius law ($\tau^{-1}=\tau_0^{-1}\exp(-\Delta/kT)+\tau_{TI}^{-1}$) (Fig. 5b).[57] The best fit provides an energy barrier $\Delta=21.5(2)$ cm^{-1}, $\tau_0=7(3)\times10^{-6}$ s) and Quantum Tunnelling of the Magnetization (QTM) at the lowest temperatures with $\tau_{TI}=3.1(1)\times10^{-3}$ s.

Computational study. In order to rationalize the magnetic observations, ab-initio calculations (SA-CASSCF/RASSI-SO) were performed on compound **1** (see Computational details). The theoretical study was performed in two steps. First, calculations were performed considering isolated Dy(III) centres, i.e. without taking into account any interaction (blue lines, Fig. S12) inducing a discrepancy between experimental and calculated data in the low-temperature range of the χ_MT vs. T plot with a calculated value of 22 cm^3 K mol^{-1} at 2K (exp.: 17.3 cm^3 K mol^{-1}). Moreover, at this stage the calculated M vs. H (at 2K) curve is characterized by a continuous increase of the magnetization along with the magnetic field without reaching saturation at 50 KOe. This behaviour may be attributed to the lack of pure axial anisotropy (Ising-type) nature of the ground state g-tensor for both Dy(III) centres, as shown in Table 2. Indeed, the ground state doublet is mainly composed of $M_J=|\pm15/2>$ (80% $M_J=|\pm15/2>$ and 16% $M_J=|\pm11/2>$) defined by a g-tensor with a main component $g_Z=18.57$ and transversal components $g_X=0.31$ and $g_Y=0.70$. The energy difference between the ground and first excited state has been calculated

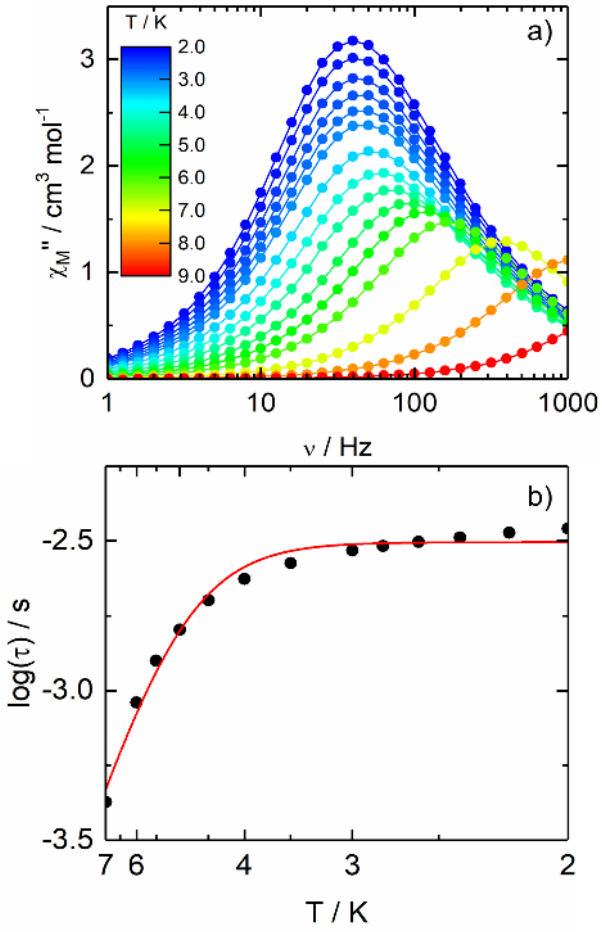

Fig 5. a) Out-of-phase component of the magnetic susceptibility for **1** between 2 and 9 K measured at 0 Oe dc magnetic field. b) Temperature dependence of the relaxation time of the magnetization with the best-fitted curve (red line) in the 2-7 K temperature range.

to be 59 K which is higher than the experimental effective value. Such overestimation is common in literature[58-63] and may be explained because ab initio model does not take into account the coupling of spin-phonon degrees of freedom in the SMM relaxation.[64,65]

Table 2. Computed energy levels (the ground state is set to zero) and decomposition of the Lande factor g for each Kramers Doublets (KD) state of the ground-state multiplet of a Dy(III) centre.

KD	Energy (cm^{-1})	g_X	g_Y	g_Z
1	0.0	0.31	0.70	18.57
2	40.9	0.63	1.45	16.42
3	95.0	0.76	1.92	13.80
4	132.5	1.36	4.33	14.64
5	164.8	0.17	4.67	10.93
6	185.6	1.95	3.54	15.59
7	221.6	0.48	1.08	16.96
8	326.3	0.01	0.02	19.41

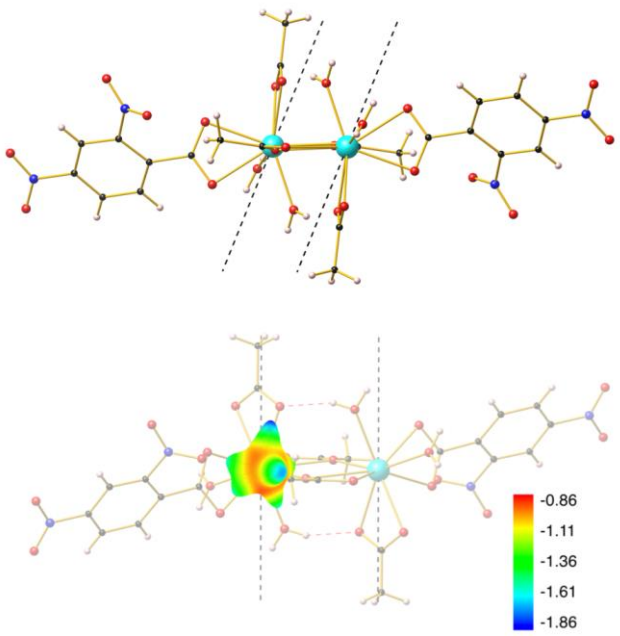

Fig 6. (Top) Orientation of the ground state g-tensor main component (g_z) calculated on each Dy centre (dark dashed lines). (Bottom) Representation of the total molecular electrostatic potential surface computed at 3 bohr from one of the magnetic centre (blue corresponds to lower potential while red stands for higher potential). The red dashed lines correspond to H-bonding between the water and acetate molecules within the dimer.

The magnetic anisotropy axis of each Dy(III) centre points towards the chelating acetate groups and makes an angle of about 65° with the plane $\{Dy_2O_2\}$ (Fig. 6). This orientation is further supported by the mapping of the molecular electrostatic potential around the magnetic centre and computed from the *ab-initio* LOPROP charge analysis[66] using the home-made CAMMEL program (see SI for a detailed description). As can be seen on Figure 6, the ground state magnetic axis tends to follow the most negative potential, pointing towards the oxygen atom from the chelating acetate group and involved in H-bonding with the water molecule from the second coordination sphere. The CAMMEL code also allows a decomposition of the total electrostatic potential into the charge, dipole and quadrupole components (Figure S13). As already pointed in previous works,[67,68] the major contribution arises from the quadrupolar term.

The observation of the transversal elements of the transition matrix shows large QTM coefficients for the ground state KD that may explain the dynamic magnetic properties of **1** (Fig. 7). The addition of dipolar interactions (J^{dip} = -0.5 cm^{-1}) within the theoretical model stabilizes the antiferromagnetic configuration leading to a non-magnetic ground state with the g-tensor components equal to zero. The ferromagnetic configuration ends up lying at about 1 cm^{-1} from the ground state with a g_z=37 (Table S4). It allows to better reproduce the decrease of $\chi_M T$ at low-temperature, ending with a value of 14.51 cm^3 K mol^{-1} at 2K (Fig. S12, green curve). Finally, an exchange contribution (J^{exch}) to the magnetic interactions is considered to fit the calculated curve to the experimental data.

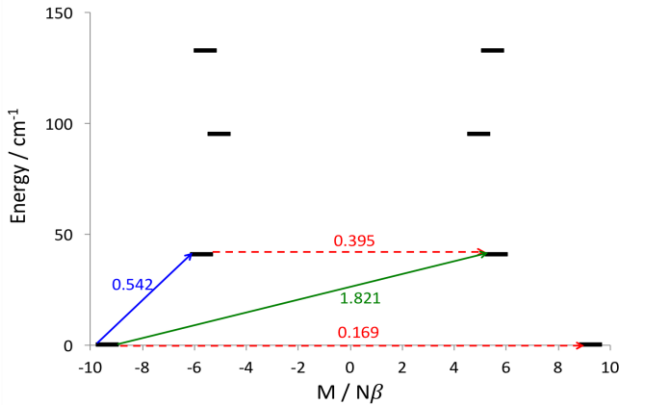

Fig 7. Relaxation pathways for each Dy centre in **1**. Black lines are Kramers doublets as a function of computed magnetic moment, red arrows are QTM/TA-QTM pathways, and green/blue arrows are Orbach/Raman relaxation pathways. The mean absolute values for the corresponding matrix element of transition magnetic dipole moment are represented with the numbers along the arrows.

The best agreement was found for J^{exch} = 0.04 cm^{-1} (Lines model) as represented in Fig. 4 and S12. These interactions might result in the quenching of the ground state QTM highlighting the zero field SMM behaviour observed for **1**.

Conclusions

To summarize, we have reported the X-ray structure of a centro-symmetric binuclear compound of Dy(III) ion involving both 2,4-dinitrobenzoate and acetate anions. The bridging (μ_2-κ^3, η^1:η^2) acetate anions transmitted small ferromagnetic exchange interactions between the Dy(III) ions while the high magnetic moments combined to the proximity of the spin carriers led to antiferromagnetic dipolar interactions. The compound behaves as a Single-Molecule Magnet in zero-applied magnetic field. The SMM thermally activated regime has an effective energy barrier for magnetization reversal around 31 K. As usual, this is slightly weaker than the energy barrier calculated from the separation between the ground and first excited states (59 K). The SMM regime is affected by quantum tunnelling at lower temperature.

Conflicts of interest

There are no conflicts to declare.

Acknowledgements

BSS thanks University Grants Commission(India) for BSR fellowship for Ph.D. GH thanks Council of Scientific and Industrial Research, India (research grant No. 01(2406)/10/EMR-II) and University Grants Commission(India) for research grant under UPE (University with potential for excellence) scheme for GNDU, for financial assistance. This work was financially supported by Région Bretagne, Rennes Métropole, CNRS, Université de Rennes 1, FEDER and the European Commission through the ERC-CoG 725184 MULTIPROSMM (project n. 725184). V. M. gratefully acknowledges the European Commission through the ERC-CoG 725184 MULTIPROSMM (project n. 725184). B.L.G. and V.M.

thank the French GENCI/IDRIS-CINES centre for high-performance computing resources.

Notes and references

1 N. Ishikawa, M. Sugita, T. Ishikawa, S. Koshihara, and Y. Kaizu, *J. Am. Chem. Soc.*, 2003, **125**, 8694-8695.
2 D. Gatteschi, R. Sessoli and J. Villain, *Molecular Nanomagnets* Oxford Univ. Press, 2006.
3 L. Bogani and W. Wernsdorfer, *Nature Mater.,* 2008, ***7***, 179–186
4 M. Mannini, F. Pineider, P. Sainctavit, C. Danieli, E. Otero, C. Sciancalepore, A. M. Talarico, M.-A. Arrio, A. Cornia, D. Gatteschi and R. Sessoli, *Nat. Mater*., 2009, **8**, 194-197.
5 J. D. Rinehart, M. Fang, W. J. Evans, J. R. Long*, J. Am. Chem. Soc.* 2011, **133**, 14263-14239.
6 S. K. Gupta, T. Rajeshkumar, G. Rajaraman, R. Murugavel, *Chem. Sci.* 2016, **7**, 5181-5191.
7 M. N. Leuenberger and D. Loss, *Nature,* 2001, **410**, 789–793.
8 J. Lehmann, A. Gaita-Arino, E. Coronado and D. Loss, *Nature Nanotech.,* 2007, **2**, 312-317.
9 M. Ganzhorn, S. Klyatskaya, M. Ruben and W. Wernsdorfer, *Nature Nanotech.,* 2013, **8**, 165-167.
10 S. Thiele, F. Balestro, R. Ballou, S. Klyatskaya, M. Ruben and W. Wernsdorfer, *Science,* 2014, **344**, 1135-1138.
11 K. S. Pedersen, A.-M. Ariciu, S. McAdams, H. Weihe, J. Bendix, F. Tuna and S. Piligkos, *J. Am. Chem. Soc*., 2016, **138**, 5801-5804.
12 C. A. P. Goodwin, F. Ortu, D. Reta, N. F. Chilton, D. P. Mills, *Nature,* 2017, **548**, 439-442.
13 F. S. Guo, M. Day benjamin, Y. C. Chen, M.-L. Tong, A. Mansikkamäki, R. A. Layfield, *Angew. Chem., Int. Ed.,* 2017, **56**, 11445-11449.
14 F.-S. Guo, B. M. Day, Y.-C. Chen, M.-L. Tong, A. Mansikkamäki, R. A. Layfield, *Science* ,2018, **362**, 1400-1403.
15 H. L. C. Feltham and S. Brooker, *Coord. Chem. Rev.*, 2014, **276**, 1-33.
16 S. R. Gupta and R. Murugavel, *Chem. Commun.,* 2018, **54**, 3685-3696.
17 J. L. Liu, Y.-C. Chen and M.-L. Tong, *Chem. Soc. Rev.,* 2018, **47**, 2431-2453.
18 G. Fernandez Garcia, D. Guettas, V. Montigaud, P. Larini, R. Sessoli, F. Totti, O. Cador, G. Pilet, and B. Le Guennic, *Angew. Chem. Int. Ed.,* 2018 DOI: 10.1002/anie.201810156.
19 F. Habib and M. Murugesu, *Chem. Soc. Rev*., 2013, **42**, 3278-3288.
20 Y. Xiaohui, K. Bernot, O. Cador, J. Luzon, G. Calvez, C. Daiguebonne and O. Guillou, *Dalton Trans.*, 2013, **42**, 6728-6731.
21 C. Y. Chow, H. Bolvin, V. E. Campbell, R. Guillot, J. W. Kampf, W. Wernsdorfer, F. Gendron, J. Autschbach, V. L. Pecoraro and T. Mallah, *Chem. Sci.,* 2015, **6**, 4148-4159.
22 X. Yi, K. Bernot, F. Pointillart, G. Poneti,, G. Calvez, C. Daiguebonne, O. Guillou, and R. Sessoli, *Chem. Eur. J*., 2012, **18**, 11379-11387.
23 F. Pointillart, Y. Le Gal, S. Golhen, O. Cador, and L. Ouahab, *Chem. Eur. J.,* 2011, **17**, 10397-10404.
24 J. D. Rineheart and J. R. Long, *Chem. Sci.*, 2011, **2**, 2078-2085.
25 Y.-M Song, F. Luo, M.-B. Luo, Z.-W. Liao, G.-M. Sun, X.-Z. Tian, Y. Zhu, Z.-J. Yuan, S.-J. Liu, W.-Y. Xu and X.-F. Feng, *Chem. Commun.*, 2012, **48**, 1006-1008.
26 D. T. Thielemann, A. T. Wagner, Y. Lan, C. E. Anson, M. T. Gamer, A. K. Powell and P. W. Roesky, *Dalton. Trans.*, 2013, **42**, 14794-14800.
27 Y.-B. Lu, X.-M. Jiang, S.-D. Zhu, Z.-Y. Du, C.-M. Liu, Y.-R. Xie and L.-X. Liu, *Inorg. Chem.,* 2016, **55**, 3738-3749.
28 F. Pointillart, B. Le Guennic, S. Golhen, O. Cador, O. Maury and L. Ouahab, *Chem. Commun*., 2013, **49**, 615-617.
29 A. B. Castro, J. Jung, S. Golhen, B. Le Guennic, L. Ouahab, O. Cador and F. Pointillart, *Magnetochemistry,* 2016, **2**, 26-37.
30 A. K. Jassal, N. Aliaga-Alcalde, M. Corbella, D. Aravena, E. Ruiz and G. Hundal, *Dalton Trans.*, 2015, **44**, 15774.
31 A. K. Jassal, B. Singh Sran, Y. Suffren, K. Bernot, F. Pointillart, O. Cador and G. Hundal, *Dalton Trans.*, 2018, **47**, 4722-4732.
32 A. Altomare, G. Cascarano, C. Giacovazzo and A. Guagliardi, *J. Appl. Crystallogr.*, 1993, **26**, 343–350.
33 G. M. Sheldrick, *Acta Crystallogr., Sect. C: Struct. Chem.*, 2015, **C71**, 3–8.
34 L. J. Farrugia, *J. Appl. Crystallogr.*, 1999, **32**, 837–838.
35 F. L. Hirshfeld, *Theoret. Chim. Acta,* 1977, **44**, 129-138.
36 S. K. Wolff, D. J. Grimwood, J. J. McKinnon, M. J. Turner, D. Jayatilaka and M. A. Spackman, Crystal Explorer ver. 3.1,University of Western Australia, Perth, Australia, (2013).
37 Y. Li, C. G. Zhang, L. Y. Cai and Z .X. Wang*, J. Coord. Chem.,* 2013, **66**, 3100-3112
38 J. J. McKinnon, F. P. A.Fabbiani , C. M. A. Spackman, Cryst. Growth Des. 2007, **7**, 755–769.
39 M. A. Spackman and D. Jayatilaka, *CrystEngComm*, 2009, **11**, 19-32.
40 F. Aquilante, J. Autschbach, R. K. Carlson, L. F. Chibotaru, M. G. Delcey, L. De Vico, I. F. Galván, N. Ferré, L. M. Frutos, L. Gagliardi, M. Garavelli, A. Giussani, C. E. Hoyer, G. L. Manni, H. Lischka, D. X. Ma, P. Malmqvist, T. Müller, A. Nenov, M. Olivucci, T. B. Pedersen, D. L. Peng, F. Plasser, B. Pritchard, M. Reiher, I. Rivalta, I. Schapiro, J. Segarra-Martí, M. Stenrup, D. G. Truhlar, L. Ungur, A. Valentini, S. Vancoillie, V. Veryazov, V. P. Vysotskiy, O. Weingart, F. Zapata, R. Lindh, *J. Comput. Chem*., 2016, **37**, 506−541.
41 B. O. Roos, P. R. Taylor, P. E. M. Siegbahn, *Chem. Phys.,* 1980, **48**, 157–173.
42 P.-A. Malmqvist, B. O. Roos and B. Schimmelpfennig, *Chem. Phys. Lett.,* 2002, **357**, 230–240.
43 P.-A. Malmqvist and B. O. Roos, *Chem. Phys. Lett.,* 1989, **155**, 189–194.
44 L. F. Chibotaru and L. Ungur, *J. Chem. Phys.,* 2012, **137**, 064112.
45 L. Chibotaru, L. Ungur and A. Soncini, *Angew. Chem., Int. Ed.,* 2008, **47**, 4126–4129.
46 L. F. Chibotaru, L. Ungur, **2006**, University of Leuven.
47 L. Ungur, W. Van der Heuvel and L. F. Chibotaru, *New J. Chem.*, 2009, **33**, 1224-1230.
48 L. F. Chibotaru, L. Ungur, C. Aronica, H. Elmoll, G. Pilet and D. Luneau, *J. Am. Chem. Soc.,* 2008, **130**, 12445-12455.
49 F. Aquilante, P.-A. Malmqvist, T. B. Pedersen, A. Ghosh and B. O. Roos, *J. Chem. Theory Comput.,* 2008, **4**, 694–702.
50 B. O. Roos, R. Lindh, P. A. Malmqvist, V. Veryazov and P. O. Widmark, *J. Phys. Chem. A.,* 2004, **108**, 2851–2858.
51 B. O. Roos, R. Lindh, P. Malmqvist, V. Veryazov, P. O. Widmark and A. C. Borin, *J. Phys. Chem. A.,* 2008, **112**, 11431−11435.
52 B. Notash, N. Safari and H. R. Khavasi, *Inorg. Chem.*, 2010, **49**, 11415-11420.
53 F. Luo, Y.-M. Song, H.-X. Huang, X.-Z. Tian, G.-M. Sun, Y. Zhu, , X.-F. Feng, *Aust. J. Chem.* 2012, **65**, 1436–1442.
54 M. S. Khiyalov, I. R. Amiraslanov, F. N. Musaev, K. S. Mamedov , *Koord.Khim. (Russ.) (Coord.Chem.)* 1982,**8**, 548.
55 O. Kahn, Molecular Magnetism, VCH, New York, 1993
56 C. Dekker, A. F. M. Arts, H. W. Wijn, A. J. van Duyneveldt and J. A. Mydosh, *Phys. Rev. B,* 1989, **40**, 11243–11251.
57 K. S. Cole and R. H. Cole, *J. Chem. Phys.,* 1941, **9**, 341–351
58 K. S. Pedersen, J. Dreiser, H. Weihe, R. Sibille, H. V. Johannesen, M. A. Sorensen, B. E. Nielsen, M. Sigrist, H. Mutka, S. Rols, J. Bendix and S. Piligkos, *Inorg. Chem.,* 2015, **54**, 7600–7606.
59 L. F. Chibotaru, L. Ungur and A. Soncini, *Angew. Chem. Int. Ed.* 2008, **47**, 4126–4129.
60 A. Lunghi and F. Totti, *Inorganics,* 2016, **4**, 28–38.

61 I. F. Diaz-Ortega, J. M. Herrera, A. R. Carmona, J. R. Galan-Mascaros, S. Dey, H. Nojiri, G. Rajaraman, E. Colacio, *Front. Chem.* DOI: 10.3389/fchem.2018.00537.
62 I. F. Diaz-Ortega, J. M. Herrera, D. Aravena, E. Ruiz, T. Gupta, G. Rajaraman, H. Nojiri, E. Colacio, *Inorg. Chem.* 2018, **57**, 6362-6375.
63 S. Mukherjee, J. Lu, G. Velmurugan, S. Singh, G. Rajaraman, J. Tang, S. K. Ghosh*, Inorg. Chem.* 2016, **55**, 11283-11298.
64 E. Lucaccini, L. Sorace, M. Perfetti, J-P. Costes, R. Sessoli, *Chem. Commun.* 2014, **50**, 1648–1651.
65 L. F. Chibotaru and L. Ungur, *J. Chem. Phys.,* 2012, **137**, 064112–064122.
66 G. Laura, L. Roland and K. Gunnar, *J. Chem. Phys.,* 2004, **121**, 4494-4500.
67 G. Huang, G. Fernandez-Garcia, I. Badiane, M. Camarra, S. Freslon, O. Guillou, C. Daiguebonne, F. Totti, O. Cador, T. Guizouarn, B. Le Guennic and K. Bernot, *Chem. Eur. J.*, 2018, **24**, 6983-6991.
68 J. Flores Gonzalez, V. Montigaud, N. Saleh, O. Cador, J. Crassous, B. Le Guennic and F. Pointillart, *Magnetochemistry*, 2018, **4**, 39.